

# Combined Energy Harvesting and Control of *Moball*: a Barycentric Spherical Robot

Joseph Bowkett, Matt Burkhardt, and Joel W. Burdick

California Institute of Technology,  
Pasadena, California 91125, USA  
[jbowkett@caltech.edu](mailto:jbowkett@caltech.edu)  
<http://robotics.caltech.edu/>

**Abstract.** The mobile sensor platform *Moball* uses an array of sliding magnets and solenoids inside a spherical shell to both harvest energy and displace its center of mass or barycenter from its center of rotation in order to control the path along which it rolls. Previous simulations of the harvesting potential for the complete system are validated experimentally, and certain phenomena that restrict effective operating conditions for energy harvesting are investigated. Tracking of characteristic trajectories for a single mass control element is used to assess the performance of the solenoids as actuators, and the ability of the system to generate a control torque during motion is demonstrated.

**Keywords:** barycentric spherical robot, *Moball*, sliding mass, solenoid actuator, energy harvesting, linear position control

## 1 Background

*Moball* (see Fig. 1) is intended to serve as a low cost wind-driven sensor platform that could be deployed in numbers to form a distributed network for taking scientific measurements over a large geographic area [1]. The Earth’s polar ice caps are of particular interest to scientists as perennial Arctic sea ice has been shown to be steadily receding, and predictive models for how this is occurring rely on data such as temperature variation, atmospheric composition, and wind velocity at ground level [2]. Most previous efforts to take such readings over large areas use remote sensing techniques such as radar backscatter signatures, but these relative methods still require absolute references of readings on the ground for accurate analysis [3]. The task of collecting such ground-truth measurements is well suited to a *Moball* network as each device would contain the necessary gas meters, thermometers, and other sensors, as well as the means to broadcast readings across the network to base stations or overhead satellites.

The windswept polar regions would also provide ample propulsive power for each system to generate and store electricity to power sensors and control its path year round, as compared to solar panel reliant systems that are inoperable during winter months.

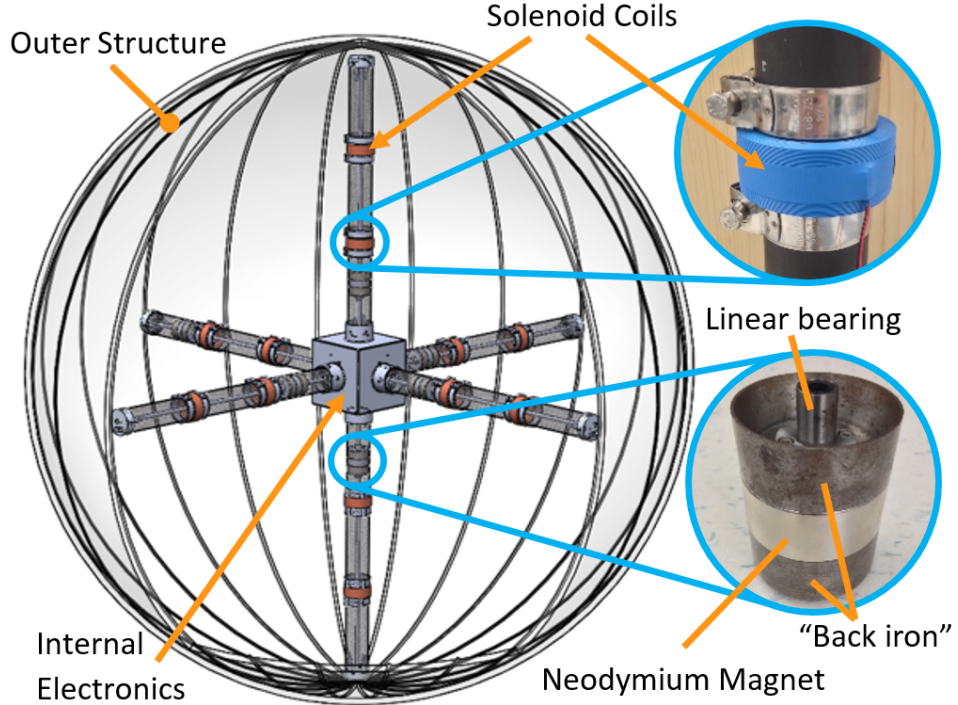


**Fig. 1.** Overview of *Moball* structure with electromagnetic components

Mars and Titan are other scientific targets where *Moball*'s ability to scavenge wind energy could allow long duration climate measurements in domains where sufficient solar energy is not realizable. Passive versions of a spherical rolling sensor platform such as the NASA/JPL *Tumbleweed* have previously been developed for use in exploring Antarctic regions or Mars [4], but as these lack any motion control they are steered solely by wind currents which may lead them away from useful measurement locations. *Moball*'s unique combination of energy harvesting and barycentric control is well suited for long duration missions in these example domains.

The *Moball* platform consists of 6 solenoidal tubes arranged radially around the center of a spherical shell composed of a nylon cladding surrounding curved fiber-glass battens that arc between the poles as shown in Fig. 1 and 2 right. Each tube has a number of solenoid coils spaced along its length and contains a specially designed mass which consists of a rare earth magnet (NdFeB) between two purpose shaped back irons. These back irons serve to redirect the magnetic field outwards from the axis of the tube increasing inductive coupling with the coil and maximizing harvested energy [5]. The system is termed barycentric because it induces motion by displacing its center of mass from its center of rotation by simultaneously coordinating the position of all 6 magnets. While the wind will provide the majority of propulsive force, barycentric control allows the vehicle to be steered in useful directions.

## 2 Energy Harvesting

When the ball moves as a result of external forces such as wind or gravity the magnets in each tube pass through their respective coils converting mechanical work into electrical energy which can be scavenged in order to power sensor electronics or be stored in batteries. This section seeks to validate simulations of the energy harvesting potential for the complete *Moball* system, and investigate any unmodeled factors that influence the maximum power that can be generated.

### 2.1 Design of Electromagnetic Components and Previous Results

Previous work on *Moball* sought to maximize the energy that can be harvested from the system by optimizing coupling between the magnet and coils as well as configuration of the coils along each tube. The FEM software JMAG was used to simulate inductive coupling for different configurations of permanent magnets and field shaping back irons finding the arrangement pictured in Fig. 1 most effective [5], using two coils equispaced 26cm from the center of the 70cm long tube. Simulations and benchtop experimental results estimated that one coil on one of the six tubes in the system can generate a peak of 1.05W when *Moball* rotates at 19rpm which is realizable in Arctic winds, with a load resistance of  $40\Omega$  as seen in Fig. 2 left.

A relationship was also found between the coil's peak power output for a given rotational velocity and the circuit's load resistance which influences the mechanical damping experienced by the magnet. Springs at the end of each tube allow some of the kinetic energy lost when the magnet reaches the end of each tube to be recovered, which extends the energy recovery capability of *Moball* to higher rotational speeds [6].

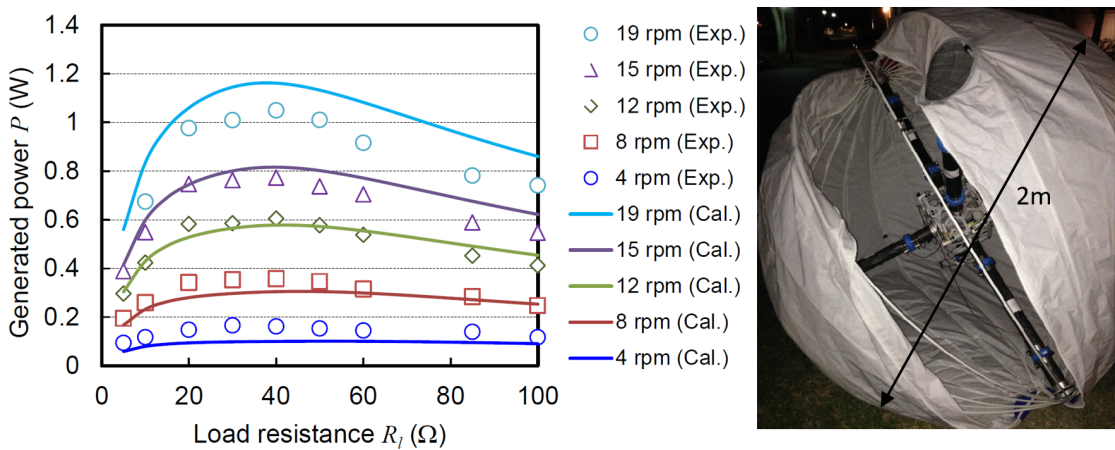


**Fig. 2.** *Left:* Comparison of simulated and experimental results for power produced by one solenoid coil at different load resistances and rotational velocities [5] *Right:* Complete *Moball* system with internals exposed through zippered shell

## 2.2 Harvesting Experimental Setup

We developed an apparatus to accurately test the energy harvesting capability of *Moball*'s solenoidal mechanism as seen in Fig. 3. The testing mechanism consists of a motor to accurately rotate the solenoidal framework, sensors to measure the operating conditions, and a custom circuit to measure energy production in real time. The axis of rotation was chosen to maximize power generation from 4 of the 6 solenoidal axes.

The power from each coil is measured from an amplified voltage over a current sense resistor in series with the load resistance for each coil. A laser distance sensor mounted within the central box allows the position of the magnet in one of the tubes to be tracked during *Moball*'s rotation. The centrally located datalogger also employs an IMU and optical sensors tripped by index markers on the frame to infer its rotation rate and orientation during each test.

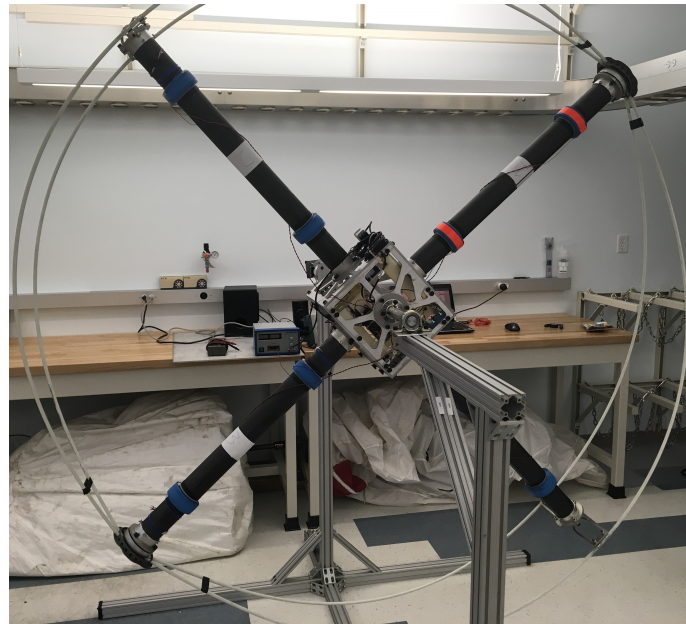


**Fig. 3.** *Moball* with most battens, one tube pair, and zippered shell (seen bottom left) removed to allow mounting on support frame

## 2.3 Validation of Harvesting Potential

The energy harvesting test apparatus was run over a range of rotation rates and load resistances. The complete results can be seen in Fig. 4. The solenoidal system produced a peak of 7.23 Watts at 20 RPM and  $47\Omega$  load resistance ( $R_L$ ). As predicted in simulation the generated power is limited at low resistances, despite the fact that the mechanical damping experienced by the magnet as it passes through each coil is highest at low load resistance.

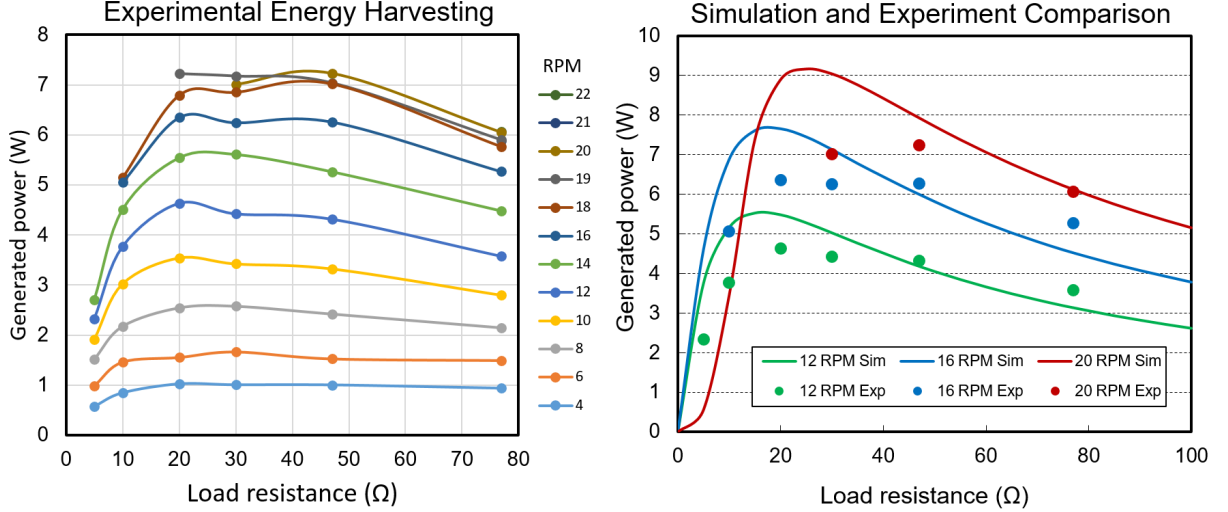


**Fig. 4.** *Left:* Complete results of measured energy harvesting potential of the entire *Moball* system *Right:* Applicable experimental results compared to simulations from Asama et al. [5]

This is thought to occur as a result of Faraday's law of induction for solenoids and power being dissipated over the coil resistance ( $R_C$ ) of  $9.5\Omega$ . The law states that the voltage induced across the coil is  $V_{coil} = \alpha(x)\dot{x}$  where  $\dot{x}$  is the velocity of the magnet and  $\alpha(x)$  is the inductive coupling between the magnet and the coil which is a nonlinear function of the distance between them. The general form of the  $\alpha$  function can be seen in Fig. 7 in Section 3. By Lenz' law this voltage potential opposes the motion of the magnet causing it to decelerate as described by Eq. (1a). At  $R_L = 5\Omega$  the inductive time constant for the harvesting circuit is 3.5ms, whereas the magnet spends 440ms within the influence of the coil resulting in negligible current transients. This allows the power over the load resistance to be approximated by Eq. (2).

$$\ddot{x} = g\sin(\theta) - \frac{\alpha(x)I}{m} \quad (a) \qquad P = \frac{1}{T} \int_0^T R_L I^2(t) dt \quad (b) \quad (1)$$

$$(R_C + R_L)I = V_{coil} - L_C(x) \frac{dI}{dt} \approx V_{coil} \quad (2)$$

When the magnet enters the  $\alpha$  function there is a spike of electrical power of which  $\frac{R_C}{R_C + R_L}$  is dissipated as heat within the coil, and this power rapidly decelerates the magnet such that the majority of its passage through the coil is at low velocity. As a result the net harvesting power described by Eq. (1b) is low for  $R_L \leq R_C$  despite the magnet losing most of its velocity to electromagnetic damping. At high load resistances the opposite effect occurs, where the majority of mechanical energy converted to electrical goes to harvesting but the total conversion is low and the magnet passes through the coil very quickly.

Previous experimental results followed the same trend as the model, though the magnitude of experimental power relative to simulated power for a single coil on one tube was shown to vary as a function of the rotation rate, as seen in Fig. 2 left. This trend was also evident on the complete system where peak experimental power was 84%, 82%, and 79% of peak simulated power for 12RPM, 16RPM, and 20RPM respectively. This is thought to be largely due to air damping of the magnet motion, as this was not accounted for in simulation. Future designs will employ vents spaced along each tube to allow air to mitigate this effect.

Air damping may also serve to explain the peak of harvesting potential appearing to occur at higher load resistances than predicted by simulation, as it slows a magnets passage through each coil therefore increasing the duration over which power is generated. This may prove advantageous as there are other benefits to harvesting with a higher load resistance as explained in Section 2.5, and will serve to allow the energy harvesting potential of the system to be optimized more accurately for intended operating conditions.

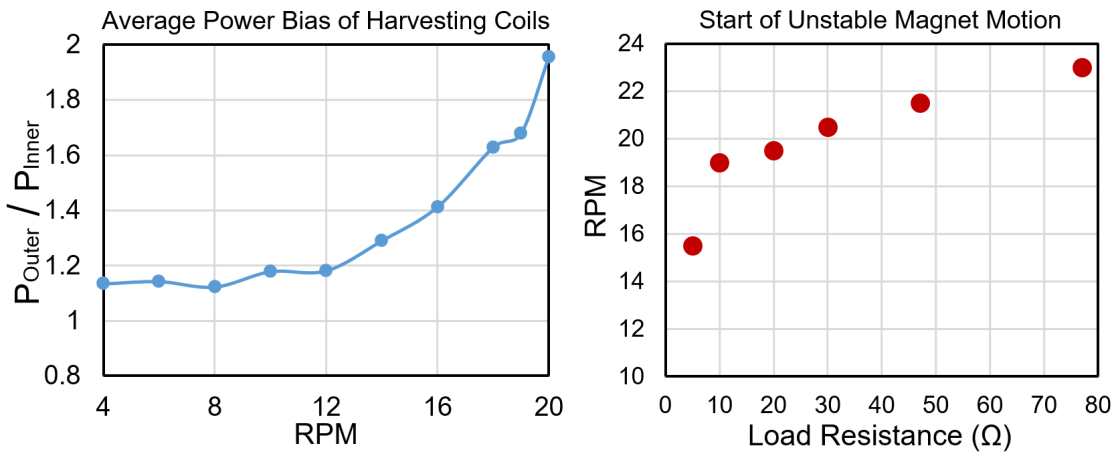


**Fig. 5.** *Left:* Normalized difference between power generated by inner and outer coils on each tube averaged across all load resistances *Right:* The speed at which the system becomes unstable and accelerates under a constant applied torque as a function of load resistance

#### 2.4 Harvesting Potential of Inner and Outer Coils

At low speeds the primary force at play pulling the magnets through the coils is gravity, however, as rotation rate increases the centrifugal force acting on the magnets begins to bias their motion towards moving away from the center of rotation. This has the effect of creating a disparity between the harvesting potential of the inner and outer coils of each tube as seen Fig. 5 left. The existing system employs identical circuitry on the inner and outer coils but the generated power may be increased by tuning the wire turns and load resistance of each to suit the magnet velocity at their respective locations under intended operating conditions.

## 2.5 Unstable Behaviour at Speed Limit

As evidenced from simulation and Fig. 4, the power generated by the system generally increases with the ball's rotation rate until the centripetal acceleration forces overcome the gravitational forces, limiting the magnet's movement through the inner coils. Asama et al. predicted this would occur around 21RPM for a load resistance of  $25\Omega$ , the peak generation for the configuration of two coils per tube. Experimental results agreed well with this value, as seen Fig. 5 right.

Simulations showed a rapid decline in peak power generation beyond this speed, however, this was difficult to replicate in testing due to a phenomena where the rotating mechanism became unstable after passing the point at which magnets cease to traverse the entire tube length. Higher speeds induce a positive feedback loop, where the rotating apparatus accelerates more rapidly as magnet travel is further reduced, diminishing the torque opposing forward motion.

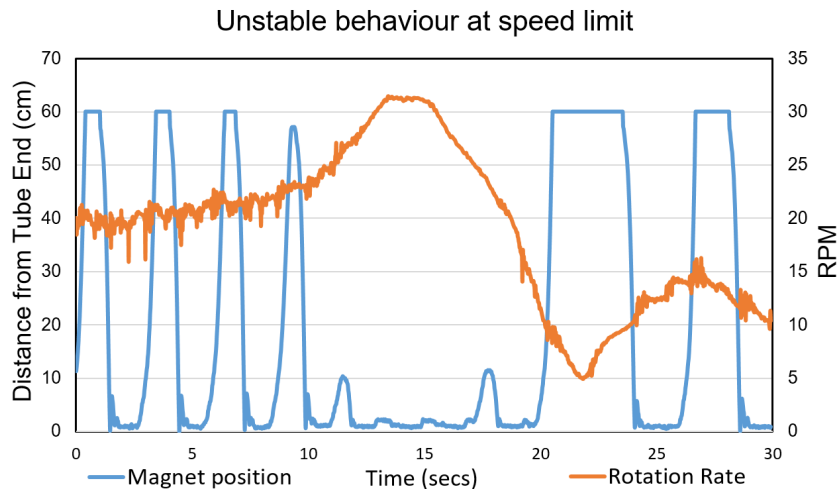


**Fig. 6.** Position of magnet in tube 3 during unstable behaviour of system at speed limit, which limits suitable operating conditions

Fig. 6 shows an example of this instability occurring in a test of  $30\Omega$  load resistance, where the blue line shows the position of the magnet in tube 3 relative to the outer end of the tube, and the orange curve shows the rotation rate of the ball. At 9 seconds the magnet does not reach the inner end of the tube and the RPM begins to increase rapidly with constant torque applied by the motor. Soon after the next rotation the magnet becomes locked at the outer tube end; the vibrations in the gyroscope signal from the impacts of the magnets at the tube ends stops as all other magnets also cease motion. At 15 seconds voltage supplied to the DC motor is reduced and the system transitions back to normal operation.

This behaviour is evidence that *Moball* design parameters must be carefully selected to avoid this unstable regime where power cannot be generated. High

speed Arctic winds can drive *Moball* at well above these speeds. Depending on the intended operating environment the ball diameter may need to be reduced in order to reduce wind force and therefore speed, as well as centripetal acceleration of the magnets (being a function of radius), to avoid entering this unstable magnet regime.

### 3 Sliding Masses as Actuators

#### 3.1 Control of Barycentric Spherical Robots

Spherical robots have long been the subject of academic study due in part to their nonholonomic constraints [7]. We model *Moball*'s motion with zero slip and zero rotation about the ground normal. Many driving mechanisms have been investigated for spherical robots, but perhaps the most common is that of barycenter offset [8]. Whether by use of an internal pendulum, sliding masses in tubes, or other means, the barycenter is displaced from the normal of the ground contact point, allowing gravity to roll the ball. Any feasible ball trajectory consisting of a 2D space of accelerations has a one to one mapping to the 2D space of net ball torques which will track it. However, as the barycenter can be positioned in three dimensions, center of mass location at any point on a given vertical line will produce the same net torque, allowing this extra dimension to be used for other design purposes such as minimizing energy expenditure. The configuration of magnet positions that produce a given barycenter location is also not unique; optimizing the mapping of desired ball path to magnet trajectories is the subject of current research beyond the scope of this paper.

The use of radially aligned sliding masses has previously been proposed as a method of barycentric control in the *Spherobot* [9], and *August* [10]. Both of these employed four masses mounted on equispaced radially aligned leadscrews driven by stepper motors, which places limits on actuation speed. By contrast, magnets driven by solenoid coils are able to traverse their entire range of motion in fractions of a second, at the expense of being more difficult to achieve precise positioning. While the centers of mass achievable by four or six equispaced radially mobile masses is similar, *Moball*'s configuration has the added benefit that when moving in a straight line under external force such as wind, two of the six coils can be actuated in order to balance and bias the direction of motion, while the remaining four are used to harvest energy.

#### 3.2 Tracking Representative Magnet Trajectories

In order to gain an appreciation of the type of magnet trajectories that may be necessary to track arbitrary paths, numerical optimization was performed on the space of magnet positions needed to achieve simple motion primitives such as moving in a straight line or following an arc of constant radius. To reduce the space of magnet positions to unique trajectories, the system center of mass was assumed to remain in a plane parallel to the ground and passing through the center of rotation, and the instantaneous velocity of each magnet minimized. These

simulations showed these magnet trajectories to be primarily comprised of sinusoids of varying frequency. It was therefore of interest to investigate the solenoid actuators' ability to track sinusoidal trajectories in the reduced system of a single tube, and understand the accuracy and speed of positioning which could be achieved.

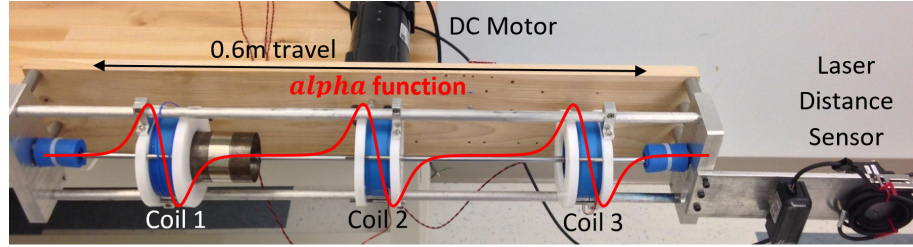


**Fig. 7.** Experimental setup for discretized magnet trajectory control, with rig mounted on DC motor to allow simulation of ball rotation. Superimposed *alpha* function describes control authority in Newtons of force applied to magnet by positive unit current through coil as a function of magnet center to coil center distance.

Due to the limited region of control authority afforded by each coil, the two coil configuration used in energy harvesting results in a control deadzone at the tube center. For this reason magnet control was implemented with three coils as seen in the experimental setup shown in Fig. 7. The solenoids are energized with a constant voltage from a 6 cell Lithium Polymer battery, controlled through a pair of H-bridge motor drivers using the duty cycle of a PWM enable signal to regulate coil current. Magnet position is again measured using a laser distance sensor, and the apparatus is rotated using the same DC motor as for energy harvesting. Preliminary tests were conducted with the tube horizontal and stationary to observe the capabilities of the actuators before adding the effects of gravity and centripetal acceleration.

Two control methods were tested for magnet positioning in order to evaluate the performance of the coils as actuators. The first employed 'bang-bang' control where coils would be energized to push the magnet towards a desired position with a fixed percentage of maximum control effort in the form of a PWM signal. This approach allowed the tracking of very aggressive trajectories such as high frequency sinusoids at the cost of using more power.

$$\ddot{x} = g\sin(\theta) - (x - x_{center})\dot{\theta}^2 + \frac{F_{coil}}{m} \quad (3)$$

The second method consisted of a proportional controller with feedback linearization. The dynamics of the magnet in a non-inertial frame attached to the tube are a function of centripetal acceleration, tube orientation  $\theta$ , gravity, and the force exerted by the coils, as described in Eq. (3) where  $x$  is position measured from one end of the tube. The electromagnetic force from each coil is  $F_{coil} = \alpha(x)I$  where  $I$  is the coil current and  $\alpha(x)$  is an inductive coupling factor which is a function of magnet to coil center distance.

To achieve feedback linearization, a model of the  $\alpha$  function developed in [5] was applied in MATLAB to the particular coil configuration used in testing, and an inverse function calculated as  $\alpha_{max}/\alpha(x)$  which when multiplied with the output of the proportional controller would approximate a linear control output. The control authority of the three coils and the alpha function can be seen in Fig. 9 left.

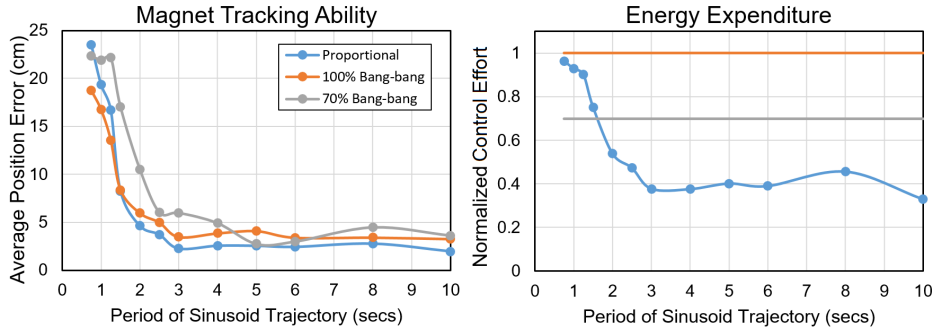


**Fig. 8.** *Left:* Measured average tracking error for different controllers across a range of sinusoidal trajectories over 60cm travel *Right:* Normalized control effort for tested controllers representing the duty cycle of PWM signal driving the control circuitry

The results of the first set of tests for tracking sinusoidal trajectories of various frequencies can be seen in Fig. 8 left. For the given testbed parameters, it is clear that tracking performance diminishes significantly at a period below 3 seconds or 20 RPM, where peak acceleration is above  $2.6m/s^2$ . Given the increase in error, the energy expended by the proportional controller attempting to track each trajectory also increases dramatically at periods below 3 seconds as seen in Fig. 8 right. As the period of the desired magnet trajectory matches that for rotation of the complete *Moball* system, this suggests that system speeds above 20RPM would be poorly controlled unless circuit parameters, in particular the applied voltage or magnet travel, were modified.

### 3.3 Demonstration of Barycentric Control

In order to demonstrate the solenoid actuator's ability to apply barycentric control to the complete system, the single tube control rig was rotated at a constant rate to simulate *Moball* rolling along a flat surface at a constant speed. Despite the numerically optimized magnet trajectories being smooth sinusoids it was found that the maximum current which could be provided by the testbed drivers was insufficient to overcome gravity at the lowest point of the  $\alpha$  function, and so a step function was employed to place the magnet at the outer tube edge on a downward stroke, the tube center when vertical, and the inner tube edge during an upward stroke. This allowed transitions between coils and regions of control authority to occur at angles where gravity could be overcome, while maximizing the net forward torque applied to *Moball* to assist its motion.

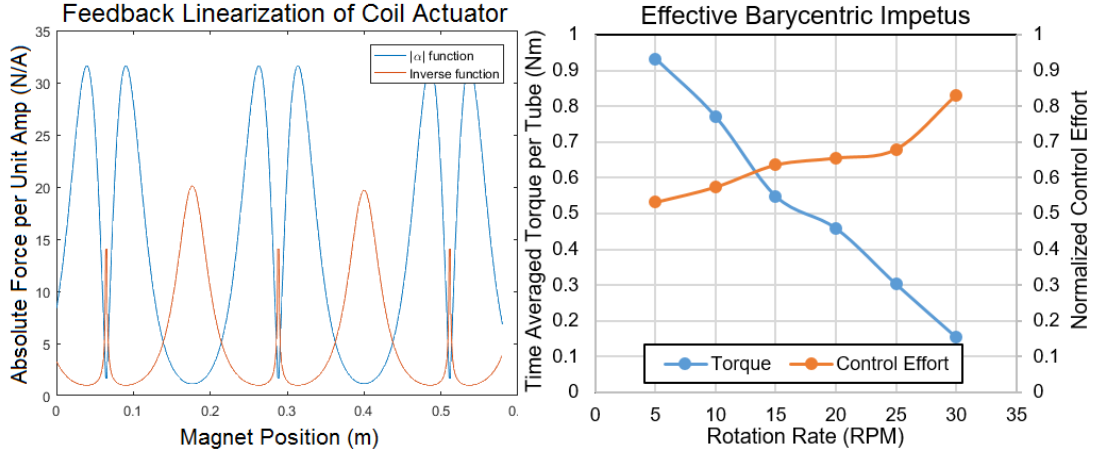


**Fig. 9.** *Left:* Absolute alpha function showing actuator authority for the given coil configuration, with inverse function used for feedback linearization *Right:* Results of test for ability of single magnet to contribute to forward motion of *Moball*

Fig. 9 right shows that the net forward torque that can be applied by each magnet reduces significantly with increasing *Moball* speed. As with tracking sinusoidal trajectories, the time spent at the end of the tube during each rotation, and therefore net torque produced by the magnet's mass effect, could be increased by raising the voltage applied to the coils. However, this would increase the power consumption necessary to maintain forward motion. Control effort also increased with RPM as seen in Fig. 9 right due in part to more frequent transfers between regions of peak control authority.

Coil current measurements proved inaccurate during control, but using the simplification of  $P = V_{max}^2/R$  suggests maximum control effort requires an upper bound of 60 Watts per tube. In practice this would be slightly below the estimated value as inductance limits the power dissipated through the coil when switching drivers cause the current to change rapidly. With the simple proportional controller employed, four tubes operating with a phase separation of  $\pi/2$  are able to produce a maximum torque of 3.72Nm at 5RPM, which requires a sustained 126 Watts. At 30RPM four tubes can produce a maximum of 0.62Nm requiring 189 Watts. The moment of inertia of the 35kg *Moball* along each primary axis is approximately  $11.75\text{kg}\cdot\text{m}^2$ .

#### 4 Conclusion and Future Work

The energy harvesting potential of the complete *Moball* system has been validated experimentally and shown to produce 7.23 Watts. Limitations on effective operating conditions have been identified and will be used to further optimize the harvesting system, which may include restructuring the tubes to form a 6-

strut tensegrity icosahedron as used in other extraplanetary rovers such as the Ames Research Center's *SUPERball* [11]. Such a configuration would increase the speeds at which *Moball* could operate before magnets become locked at the outer edge by reducing the distance of tube ends from their orthogonal rotation axes therefore reducing peak centripetal acceleration. This would also extend magnet travel and increase the range of centers of mass achievable for control.

Barycentric control using a single mass element has been demonstrated, and the power requirements for sustained controlled motion of the complete system using a proportional magnet controller estimated to be on the order of 130W. While sustained maximum control effort is not the intended use for the system, being more suited to biasing motion than creating it, current work seeks to reduce this figure by employing impulse controllers to only apply power when a magnet is in the peak of the  $\alpha$  function, increasing actuator energy efficiency.

## References

1. Davoodi, F., Burdick, J.W., Rais-Zadeh, M.: Moball Network: A Self-Powered Intelligent Network of Controllable Spherical Mobile Sensors to Explore Solar Planets and Moons. In: AIAA SPACE 2014 Conference and Exposition, pp. 1–9 (2014)
2. Dry, S.J., Yau, M.K.: Large-scale mass balance effects of blowing snow and surface sublimation. *Journal of Geophysical Research: Atmospheres* 107(D23), ACL 8-1–ACL 8-17 (2002)
3. Nghiem, S.V., Clemete-Colon, P.: Arctic sea ice mapping with satellite radars. In: Radar Conference, 2008. RADAR '08. IEEE, pp. 1–3 (2008)
4. Southard, L., Hoeg, T.M., Palmer, D.W., Antol, J., Kolacinski, R.M., Quinn, R.D.: Exploring Mars Using a Group of Tumbleweed Rovers. In: Robotics and Automation, 2007 IEEE International Conference on, pp. 775–780 (2007)
5. Asama, J., Burkhardt, M.R., Davoodi, F., Burdick, J.W.: Design investigation of a coreless tubular linear generator for a Moball: A spherical exploration robot with wind-energy harvesting capability. In: Robotics and Automation (ICRA), 2015 IEEE International Conference on, pp. 244–251 (2015)
6. Burkhardt, M.R., Davoodi, F., Burdick, J.W., Davoudi, F.: Energy harvesting analysis for Moball, A self-propelled mobile sensor platform capable of long duration operation in harsh terrains. In: Robotics and Automation (ICRA), 2014 IEEE International Conference on, pp. 2665–2672 (2014)
7. Johnson, B.D.: The Nonholonomy of the Rolling Sphere. *American Mathematical Monthly* 114(6), 500–508 (2007)
8. Chase, R., Pandya, A.: A Review of Active Mechanical Driving Principles of Spherical Robots. *Robotics* 1(1), 3 (2012)
9. Mukherjee, R., Minor, M.A., Pukrushpan, J.T.: Simple motion planning strategies for spherobot: a spherical mobile robot. In: Decision and Control, 1999. Proceedings of the 38th IEEE Conference on, 2132–2137 vol.3 (1999)
10. A, A.H.J., Mojabi, P.: Introducing August: a novel strategy for an omnidirectional spherical rolling robot. In: Robotics and Automation, 2002. Proceedings. ICRA '02. IEEE International Conference on, 3527–3533 vol.4 (2002)
11. Bruce, J., Caluwaerts, K., Iscen, A., Sabelhaus, A.P., SunSpiral, V.: Design and evolution of a modular tensegrity robot platform. In: 2014 IEEE International Conference on Robotics and Automation (ICRA), pp. 3483–3489 (2014)